

# Dalton Transactions

Accepted Manuscript



This is an *Accepted Manuscript*, which has been through the Royal Society of Chemistry peer review process and has been accepted for publication.

*Accepted Manuscripts* are published online shortly after acceptance, before technical editing, formatting and proof reading. Using this free service, authors can make their results available to the community, in citable form, before we publish the edited article. We will replace this *Accepted Manuscript* with the edited and formatted *Advance Article* as soon as it is available.

You can find more information about *Accepted Manuscripts* in the [Information for Authors](#).

Please note that technical editing may introduce minor changes to the text and/or graphics, which may alter content. The journal's standard [Terms & Conditions](#) and the [Ethical guidelines](#) still apply. In no event shall the Royal Society of Chemistry be held responsible for any errors or omissions in this *Accepted Manuscript* or any consequences arising from the use of any information it contains.

## ARTICLE

# Design of UV-Vis-NIR Panchromatic Crown-Phthalocyanines with Controllable Aggregation

Cite this: DOI: 10.1039/x0xx00000x

Evgeniya A. Safonova,<sup>a</sup> Alexander G. Martynov,<sup>\*a</sup> Viktor I. Zolotarevskii,<sup>a</sup> Sergey E. Nefedov,<sup>b</sup> Yulia G. Gorbunova,<sup>\*a,b</sup> and Aslan Yu. Tsivadze<sup>a,b</sup>Received 00th January 2012,  
Accepted 00th January 2012

DOI: 10.1039/x0xx00000x

[www.rsc.org/](http://www.rsc.org/)

Novel magnesium and zinc phthalocyaninates, bearing four lateral electron-rich 15-crown-5-oxanthrene fragments, were synthesized starting from benzo-15-crown-5. Being almost insoluble in common organic solvents, these complexes could be solubilised by means of interaction with potassium acetate – due to formation of well-defined cofacial supramolecular dimers. Characteristic feature of these dimers is the presence of additional band in their UV-Vis spectra, which affords expansion of light absorption region up to ~750 nm. This new band corresponds to charge transfer from peripheral groups to Pc core, as evidenced by TDDFT calculations. Potassium cations can be reversibly removed from these dimers by [2.2.2]cryptand, resulting in formation of monodisperse nanoparticles with absorbance up to 900 nm. This approach can be further used for fabrication of nanostructured optoelectronic materials, based on synthesized donor-acceptor panchromatic crown-phthalocyanines.

## Introduction

Conjugation of phthalocyanines (Pcs) with lateral aromatic groups is known to have crucial effect on their properties and, therefore, functional characteristics of optoelectronic materials on their basis. Such structural modification results in expansion of  $\pi$ -system, leading to contraction of HOMO-LUMO gap.<sup>1,2</sup> In turn, it causes bathochromic shift of the Q-band to near-IR region together with decrease of oxidation potentials. Resulting NIR-absorbing pigments are prominent photosensitizers for various applications, including solar energy conversion, photodynamic therapy, nonlinear optics, etc.<sup>3</sup>

On the other hand, expansion of Pcs aromatic system leads to enhanced aggregation due to intermolecular  $\pi$ -stacking interactions.<sup>4</sup> The effect of aggregation can be considered either as negative, or positive, depending on required functionality of materials. For example, quenching of Pcs luminescence is a known side-effect of aggregation which is undesired for medical applications.<sup>5</sup>

Such aggregation may be prevented by introduction of bulky substituents like *tert*-butyl-,<sup>6</sup> 2,6-dialkylphenoxy-,<sup>7</sup> etc. on the periphery of Pc macrocycle. On the other hand, formation of aggregates is a key point in development of OFET's, bulk heterojunction solar cells and other optoelectronic materials and devices, where these aggregates conduct excitons.<sup>8</sup> Therefore, control over aggregation of Pcs is an important task, and much attention is paid to systems, where external stimuli can cause reversible switching between aggregated and disaggregated

forms. Among them, the most well known Pc molecules with controllable aggregation are crown-substituted phthalocyanines and their complexes.<sup>9–12</sup> Addition of alkali metal cation with size exceeding crown-ether cavity to solutions of crown-Pcs is known to result in formation of well-defined aggregates with architecture, depending on the nature of receptor – crown-Pc and substrate – metal salt (both cation and anion).<sup>13–17</sup>

Moreover, similarly to many other phthalocyanines, under certain conditions crown-substituted Pcs are capable of self-assembling in solution with the formation of different aggregates – starting from dimers to supramolecular wires with hundreds nm length.<sup>18–20</sup> For example, it was demonstrated that Ru(II) tetra-15-crown-5-phthalocyaninates with axially coordinated ligands (DABCO, ethyl-*iso*-nicotinate, etc.), being added to conducting polyimide, form photorefractive composites with performance in NIR range.<sup>21,22</sup> This becomes possible due to the fact that the Pc molecules form supramolecular aggregates with brickwork-like architecture, providing growth of absorbance in NIR region together with efficient enhancement of nonlinear optical susceptibility.<sup>23,24</sup> The role of crown-ethers in formation of such supramolecular assemblies was suggested, basing on X-ray diffraction data.<sup>25–27</sup>

Herein we report synthesis and properties of novel Pcs bearing 15-crown-5-oxanthrene groups on the examples of magnesium and zinc complexes **8Mg** and **8Zn** (Fig. 1) which are proposed to be called as tetra-(15-crown-5-oxanthrene)-phthalocyanines.

Design of such systems was based on several assumptions:

-Introduction of electron-donating tetra-oxy-benzene units coplanar with Pc core can result in their efficient conjugation through bridging  $sp^2$ -O atoms, leading to expansion of aromatic system and hypsochromic shift of Q-band to NIR.

-Lateral expansion of Pcs molecule with aromatic groups can increase tendency to aggregation, which in turn can be triggered by interaction with alkali-metal ions.

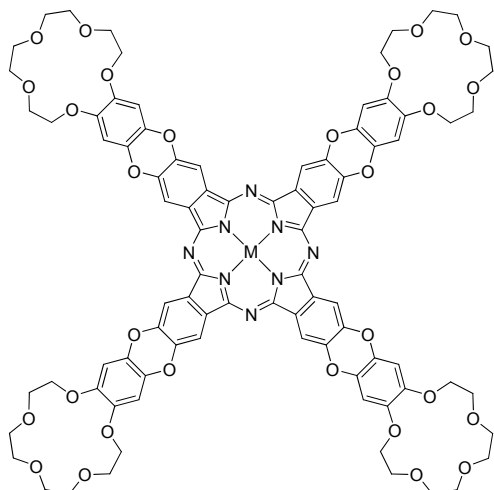


**Fig. 1.** Tetra-(15-crown-5-oxanthreno)-phthalocyanine **8**, M=Mg and Zn (**8Mg** and **8Zn**, respectively).

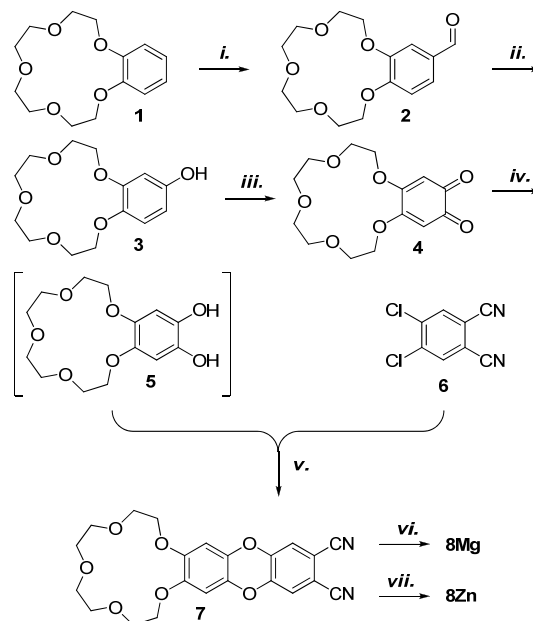
## Results and discussion

Broadening of UV-Vis absorption range of Pcs is typically attained either by expansion of aromatic system (for example, by synthesis of naphthalocyanines or their heterocyclic analogues, etc.), or by introduction of strong electron donors. With this aim we have firstly proposed novel type of electron-donating substituent, namely tetra-oxy-benzene units conjugated with Pc core. Molecules, bearing this electron-rich fragment, are known to form complexes with electron acceptors.<sup>28,29</sup>

Synthesis of Pcs **8Mg** and **8Zn** required preparation of corresponding precursor – oxanthrenodinitrile **7**, bearing 15-crown-5-macrocycle. Retrosynthesis of **7** suggested that it can be prepared by nucleophilic substitution of chlorine atoms in 4,5-dichlorophthalonitrile by corresponding crown-substituted catechol.<sup>30–32</sup> While the first reagent is commercially available, synthesis of 15-crown-5-catechol was not reported previously. Its synthesis was performed starting from commercially available benzo-15-crown-5 **1** (Scheme 1).

Formylation of **1** by mixture of  $\text{POCl}_3$  and *N*-methylformamide afforded 15-crown-5-benzaldehyde **2**, which was subsequently deformylated with simultaneous hydroxylation (Baeyer–Villiger oxydation/rearrangement). Oxidation of resulting phenol **3** with Fremy's salt<sup>33</sup> in dihydrophosphate buffer solution afforded 15-crown-5-substituted *o*-quinone **4** – novel compound, which itself can be

attractive ligand for further synthesis of new ionophoric redox-active complexes.



**Scheme 1.** Synthesis of phthalonitrile **7**. Reaction conditions: *i.*  $\text{PhN}(\text{Me})(\text{COH})$ ,  $\text{POCl}_3$ ,  $75^\circ\text{C}$ , 3 h, yield – 74%. *ii.* 30% aq.  $\text{H}_2\text{O}_2$ , conc.  $\text{H}_2\text{SO}_4$ , MeOH, RT, 12 h, yield – 79%. *iii.* Fremy's salt,  $\text{KH}_2\text{PO}_4$ ,  $\text{H}_2\text{O}$ , MeOH,  $0^\circ\text{C}$ , 1.5 h, yield – 57%. *iv.*  $\text{H}_2$ , Pd/C, DMF, RT, 2 h (without isolation). *v.*  $\text{K}_2\text{CO}_3$ , DMF,  $70^\circ\text{C}$ , 18 h, Ar, yield – 81%. *vi.*  $\text{Mg}(\text{OAc})_2$ , DBU, *i*-AmOH, reflux, 15 h, Ar, yield – 81%. *vii.*  $\text{Zn}(\text{OAc})_2$ , DBU, *i*-AmOH, reflux, 15 h, Ar, yield – 57%.

Reduction of quinone **4** into corresponding catechol **5** could be performed under different conditions, among them – previously reported reduction with  $\text{Na}_2\text{S}_2\text{O}_4$  in aqueous media, which was used, for example, for reduction of similar benzo[1,3]dioxole-5,6-dione.<sup>29</sup> However, attempt to use this reaction in our case resulted in formation of insoluble precipitate, which could not be characterized. Thus, we applied hydrogenolysis reaction in EtOAc, using 10% Pd/C catalyst. Indeed, it resulted in reduction of bright orange quinone **4** with the formation of colourless catechol **5**, which however reoxidized into quinone **4** upon filtration and evaporation of the solvent as evidenced by NMR. To use catechol **5** for the next step without isolation, we performed hydrogenolysis in anhydrous DMF until orange colour of quinone vanished. Then, reaction mixture was filtered through syringe filter to remove Pd/C catalyst. Colourless filtrate was transferred into flask, containing dichlorophthalonitrile **6** and  $\text{K}_2\text{CO}_3$  in DMF. Performing this reaction under strictly inert atmosphere afforded target oxanthrene **7** as a yellow powder in 81% yield. All intermediates were characterized by standard set of physical-chemical methods, including X-ray diffraction analysis, performed for phthalonitrile **7** (Fig. 2). Its single crystals, suitable for X-ray diffraction analysis, were obtained by slow evaporation of solution of **7** in  $\text{CH}_2\text{Cl}_2/\text{MeOH}$  (9:1 vol.) mixture.

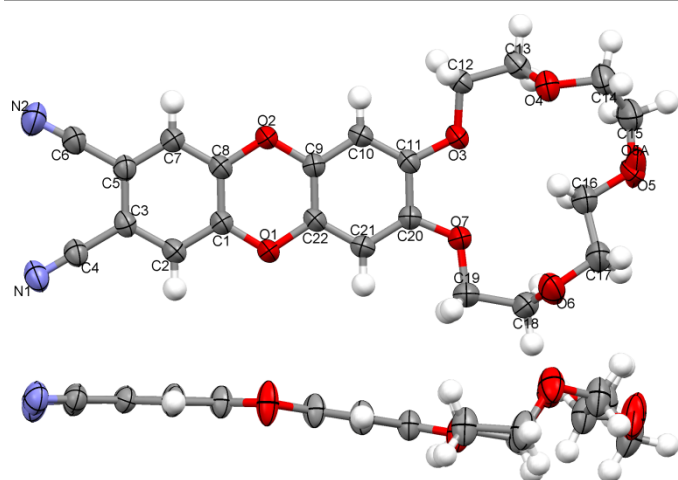


**Fig. 2.** Molecular structure of **7** with thermal ellipsoids drawn at the 50% probability level. Benzene rings, containing electron-acceptor cyano-groups and electron-donating crown-ether ring are signed as **A** and **D** for further discussion. Carbon atoms C(3) and C(5) in *ipso*-positions to cyano-groups, will be referred as  $C_A$ ; C(11) and C(20) in *ipso*-positions to crown-ether – as  $C_D$ .

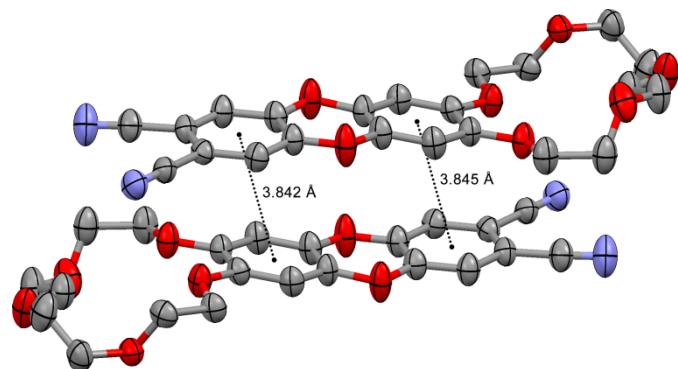


**Fig. 3.** Head-to-tail dimer, formed by nitrile **7** in crystal. Hydrogen atoms are omitted for clarity.

Analysis of structure evidences that oxanthrene core is slightly bent – dihedral angle between planes of benzene rings **A** and **D** is  $7.64^\circ$ , while parent dibenzo-*p*-dioxine is known to be flat.<sup>34</sup> Such deviation from planarity is likely to provide dense molecular packing of bulky 15-crown-5 group. This can be indirectly supported by DFT B3LYP/6-31G(d) geometry optimization, performed for the single molecule of **7** in vacuum. Such optimization results in flattening of oxanthrene fragment. The structure reveals notable alterations of lengths of chemical bonds between oxygen atoms of dioxin ring and carbon atoms of benzene rings **A** and **D** (Table 1). Bond lengths  $C_A-O_{\text{dioxin}}$  are by  $\sim 0.03\text{Å}$  longer than  $C_D-O_{\text{dioxin}}$ . For comparison, unsubstituted oxanthrene has intermediate C-O bond length. The values of  $C_A-O_{\text{dioxin}}$  are close to bond lengths between oxygen atom of crown-ether and carbon atom of the benzene ring **D**. The same trends in C-O bend length alteration are reproduced in DFT-optimized structure of **7**. Calculated Löwdin bond orders of C-O bonds are as follows:  $C_A-O_{\text{dioxin}} - 1.21$ ,  $C_D-O_{\text{dioxin}} - 1.13$ ,  $C_D-O_{\text{crown}} - 1.24$ .

Molecules of **7** from head-to-tail dimers (Fig. 3), with average intermolecular separation between centroids of donor

and acceptor rings, equal to  $3.842\text{--}3.845\text{Å}$ . It is by  $\sim 0.4\text{Å}$  larger than molecule-to-molecule separation observed in 1:1 crystal of dibenzo-*p*-dioxin and tetracyanoquinodimethane.<sup>28</sup>

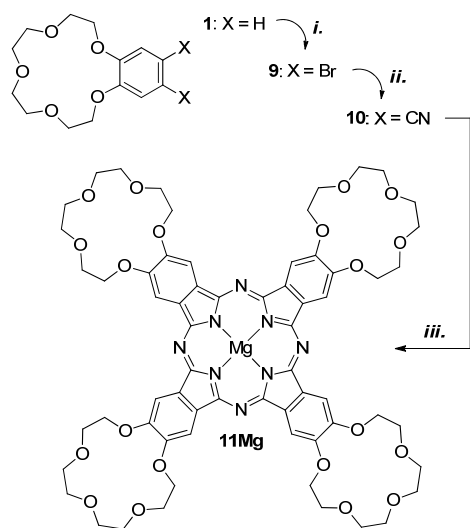
Table 1. Selected C-O bond lengths in X-ray structure of **7**.

Bond	Bond length, Å
$C_A-O_{\text{dioxin}}$	
C(1)-O(1)	1.3661(18)
C(8)-O(2)	1.3678(18)
$C_D-O_{\text{dioxin}}$	
C(22)-O(1)	1.3982(18)
C(9)-O(2)	1.3821(18)
$C_D-O_{\text{crown}}$	
C(11)-O(3)	1.3576(17)
C(20)-O(7)	1.3603(18)
C-O in dibenzo- <i>p</i> -dioxin	1.383(8) <sup>34</sup>

Reaction of nitrile **7** with anhydrous  $\text{Zn}(\text{OAc})_2$  in refluxing *i*-AmOH in the presence of DBU was followed by appearance of dark green colour, and in course of reaction formation of dark precipitate was observed. This was assigned to formation of target complex – **8Zn** on the basis of MALDI TOF mass-spectra of reaction mixture sample. Extraction of low-molecular impurities with EtOH afforded dark-green powder, which however was almost insoluble in common organic solvents, like  $\text{CHCl}_3$ , DMF, DMSO, pyridine. Low solubility **8Zn** is likely to be caused by intermolecular interactions between electron-donating tetra-oxy-benzene groups and electron-accepting Pc core, similarly to stacking interactions, which were observed in dimer, formed by **7** in crystal.

With the idea to prepare more soluble compound, which could be studied in solution, magnesium complex **8Mg** was synthesized, assuming high tendency of magnesium Pcs to coordinate various axial ligands, which could hinder intermolecular interactions. Indeed, **8Mg** turned out to be soluble in mixture of  $\text{CHCl}_3$  with MeOH. Notably, in the absence of methanol complex remained insoluble in  $\text{CHCl}_3$ . All further studies of **8Mg** in solution were performed in  $\text{CHCl}_3$ , containing 10vol.% of MeOH.

Well-soluble magnesium tetra-15-crown-5-phthalocyaninate **11Mg** was synthesized as a reference compound by template condensation of dicyanobenzo-15-crown-5 **10** in the presence of  $\text{Mg}(\text{OAc})_2$  and DBU in refluxing *i*-AmOH (Scheme 2). For preparation of phthalonitrile **10** bromination of benzo-15-crown-5 **1** with NBS and subsequent Pd-catalyzed cyanation were applied, which afforded increase of overall yield and significantly simplified isolation procedures in comparison with Rosenmund-Braun cyanation.<sup>35,36</sup>



**Scheme 2.** Synthesis of tetra-15-crown-5-phthalocyanine **11Mg**. Reaction conditions: *i.* NBS,  $\text{CHCl}_3$ , reflux, 5 h, yield – 80%. *ii.*  $\text{Zn}(\text{CN})_2$ ,  $\text{Pd}_2(\text{dba})_3$ , dppf, DMAA,  $120^\circ\text{C}$ , 2.5 h, Ar, yield – 81%. *iii.*  $\text{Mg}(\text{OAc})_2$ , DBU, *i*-AmOH, reflux, 24 h, Ar, yield – 61%.

UV-Vis spectrum of **8Mg**, dissolved in  $\text{CHCl}_3/\text{MeOH}$  mixture revealed split Q-band with *two* maxima at 686 and 639 nm. At the same time, reference complex **11Mg** exhibited only *one* Q-band with maximum at 680 nm. It was very tempting to associate the splitting and bathochromic shift of Q-band's maximum of complex **8Mg** with expansion of aromatic system due to introduction of oxanthrene units – the effect which was anticipated at the beginning of this work. However, when dynamic light scattering measurements of this solution were performed, it was demonstrated that **8Mg** forms colloidal solution, containing particles with average hydrodynamic radius 13.7 nm (Fig. 4). Therefore, it was not correct to compare UV-Vis spectra of aggregated **8Mg** with monomeric **11Mg**, which revealed no light scattering.

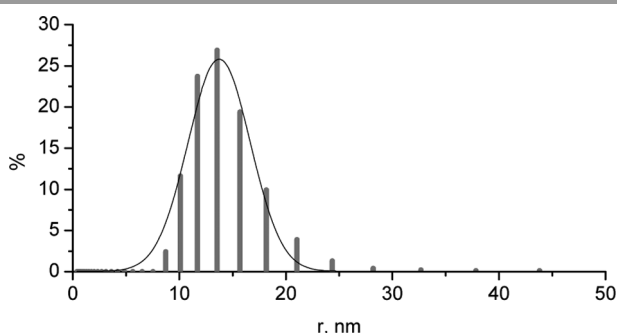


**Fig. 4.** Profile of particle size distribution obtained by DLS measurements for colloidal solution of  $\text{Mg}[(15\text{C}5\text{Ox})_4\text{Pc}]$  ( $2 \cdot 10^{-5}$  M in  $\text{CHCl}_3 + 10$  vol.% MeOH). Average hydrodynamic radius – 13.7 nm.

Previously, we have proposed the way to control solubility of ZnPc complex, bearing four lateral 1,10-phenanthroline-containing rings.<sup>37</sup> Being totally insoluble itself, this complex could be solubilised by interaction with  $\text{Cu}^+$  ions, which resulted in destruction of aggregates and formation of monomeric species in solution. Obviously, this powerful

approach can be used in the present case, due to the presence of crown-ether units in molecules of **8Mg** and **8Zn**, which are well-known ligands for alkali metal ions. Herein, KOAc was used as a solubilising agent – it was expected that complexes would form eclipsed supramolecular dimers similarly to other comprehensively studied square-planar and pyramidal crown-Pcs.<sup>9</sup>

For reference, complex **11Mg** was also treated with KOAc in  $\text{CHCl}_3 + 10$  vol.% MeOH mixture. Titration process was followed by decrease of Q-band's intensity, followed by growth of *one* new hypsochromically shifted band at 636 nm (Fig. 5a,b). The slope of titration curves approached to zero after addition of 2 equivalents of KOAc. These spectral changes are characteristic for formation of well-defined supramolecular dimer  $(\mathbf{11Mg})_2(\text{KOAc})_4$  with cofacial architecture, similarly to previously studied square-planar crown-Pcs, like zinc tetra-15-crown-5-phthalocyanine.<sup>14</sup>

Spectrophotometric titration of colloidal solution of **8Mg** also resulted in interaction between complex and KOAc, which was accomplished after addition of 2 equivalents of KOAc (Fig. 5c,d). This interaction was followed by small hypsochromic shift of both components of Q-band region. Clear isobestic points were observed in course of titration. The observed shift was not as spectacular, as in the case of **11Mg** probably because the starting complex already exists in aggregated state. However, the most characteristic feature of the resulting spectrum is that in the Q-band region still contains *two* bands with maxima at 637 and 674 nm. Notably, resulting solution did not exhibit any light scattering.

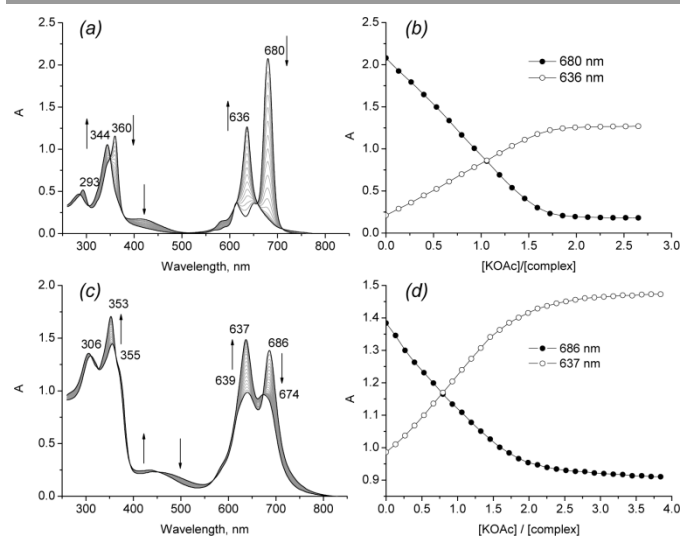


**Fig. 5.** Changes of UV-Vis spectra upon titration of **11Mg** (a) and **8Mg** (c) in  $\text{CHCl}_3 + 10$  vol.% MeOH mixture with KOAc solution in MeOH together with corresponding titration curves (b) and (d), plotted at maxima of Q-bands.

To unravel the architecture of the resulting supramolecular assemblies, their NMR investigation was performed (Fig. 6). It confirmed that these species are cofacial dimers  $(\mathbf{8Mg})_2(\text{KOAc})_4$ , similar to the ones, formed by **11Mg**. This conclusion was drawn because of characteristic splitting of resonance signals of crown-ether  $\text{CH}_2$ -groups due to

nonequivalence of *exo*- and *endo*-protons with respect to the space between Pc molecules.<sup>38</sup> At the same time, only two singlets were observed in aromatic region, corresponding to Pc protons and protons of tetra-oxy-benzene ring. It suggests that high symmetry of molecule is preserved in supramolecular assembly, otherwise, more complicated pattern would be observed, similarly to NMR spectra of triple-decker REE(III) phthalocyaninates.<sup>26,39–41</sup> Schematic representation of dimeric architecture, formed by **8Mg** is given in Fig. 7.

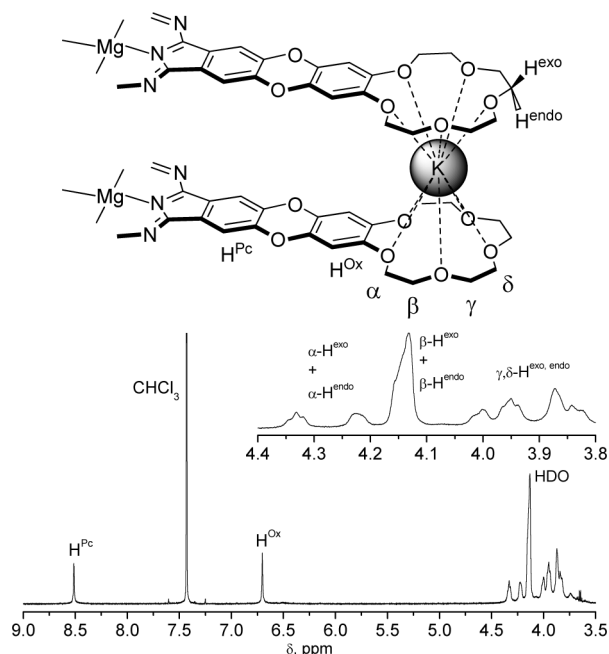


**Fig. 6.** NMR spectrum of supramolecular dimer, formed by **8Mg** in the presence of potassium ions in  $\text{CDCl}_3/\text{CD}_3\text{OD}$  mixture. Assignment of protons is given above.

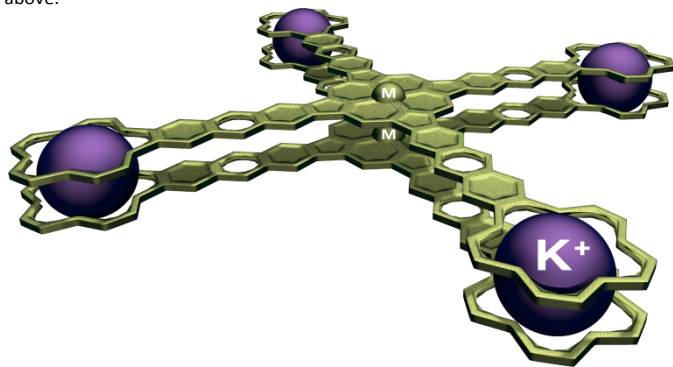


**Fig. 7.** Schematic representation of architecture of supramolecular dimer, formed by **8Zn** in the presence of potassium ions.

The described supramolecular approach was also used to solubilise zinc complex **8Zn**. With this aim, its suspension in  $\text{CHCl}_3+10\text{vol.}\% \text{MeOH}$  mixture was treated with 2 equivalents of KOAc. It resulted in dissolving of almost black solid with the formation of clear green solution within  $\sim 1$  h. The process was followed by growth of *two* bands in Q-band region (Fig. 8). This analogy of spectral behaviour of **8Mg** and **8Zn** in the presence of KOAc can evidence of formation of supramolecular dimer in the later case as well.

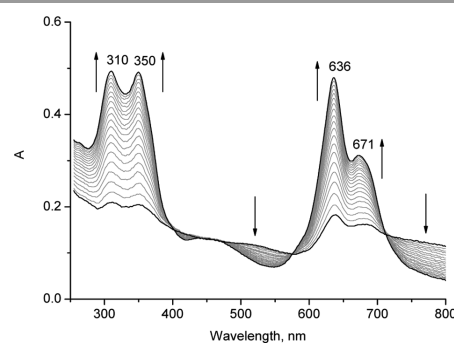


**Fig. 8.** Changes in UV-Vis spectrum of **8Zn** upon its dissolution in the presence of KOAc in  $\text{CHCl}_3+10\text{vol.}\% \text{MeOH}$  mixture within 1h.

Therefore, we can correctly compare UV-Vis spectra of well-defined supramolecular dimers, formed by **8M** and **11M**,  $\text{M}=\text{Mg}, \text{Zn}$ . The comparison evidences, that expansion of Pc aromatic system due to introduction of 15-crown-5-oxanthrene fragments results in appearance of additional intensive band in UV-Vis spectra at 670-675 nm. This band is relatively broad and its long-wavelength side covers region up to 750 nm.

In the case of Pc metal complexes, dominant light absorption in visible region is the Q-band, which corresponds to HOMO $\rightarrow$ LUMO transition. Both these orbitals are localized mainly on Pc core.<sup>42</sup> Since new band in UV-Vis spectra of dimers, formed by **8Mg** and **8Zn** is associated with introduction of 15-crown-5-oxanthrene group, it looks reasonable that this new band can correspond to charge transfer (CT) from electron-rich periphery to Pc, acting as electron acceptor.

To confirm CT origin of this band, we have performed DFT/TDDFT calculations for model compounds – monomeric octa-methoxy-substituted complex  $\text{Mg}[(\text{MeO})_8\text{Pc}]$ , intermediate oxanthrene-substituted  $\text{Mg}[(\text{Ox})_4\text{Pc}]$  and finally, prototype of **8Mg** –  $\text{Mg}[(\text{MeO}_2\text{Ox})_4\text{Pc}]$ .

Calculations of dimeric species could not be performed at the currently available computational facilities because of large size of such systems. However, the well-known correlations between spectra of monomeric and dimeric Pcs, based on Kasha's exciton theory,<sup>43</sup> can be used to draw required conclusions. Numerous experimental evidences were obtained which confirm this theory for spectral behaviour of Pcs upon aggregation.<sup>4</sup> Theoretical validation of this model was also performed at B3LYP/6-31G\* level of theory, which confirmed that cofacial dimerization of Pc molecules leads to hypsochromic shift of the Q-band without appearance of new spectral bands.<sup>44</sup>

Calculations were performed using ORCA 2.9.1 software.<sup>45</sup> Optimized structures were obtained by BP86/TZV calculations. Previously, on the example of ZnPc it was demonstrated that the TDDFT-calculated vertical excitation energies correlate with the amount of Hartree-Fock exchange involved in the applied exchange-correlation functional.<sup>46</sup> To choose the applicable functional for our studies, we have tested pure BP86 and hybrid B3LYP exchange-correlation functionals with 0% and 20% HF exchange respectively. BP86 failed to predict UV-Vis spectrum of  $\text{Mg}[(\text{MeO})_8\text{Pc}]$  – instead of one essentially

pure HOMO-LUMO transition for Q-band it suggests three transitions in Q-bands region with significant contribution of transitions from low-lying occupied MOs to LUMO. In the case of B3LYP/6-31G(d) TDDFT calculations the appearance of single band in Q-band region was predicted, which correlates well with experimental data. Although it is known, that B3LYP/6-31G(d) TDDFT calculations overestimate energy, corresponding to Q-band's transition by  $\sim 0.3$  eV,<sup>47</sup> they give qualitatively acceptable trends for further comparative analysis, therefore, this level of theory is used in the present work. Diagram of frontier orbitals of three investigated molecules is given in Fig. 9.

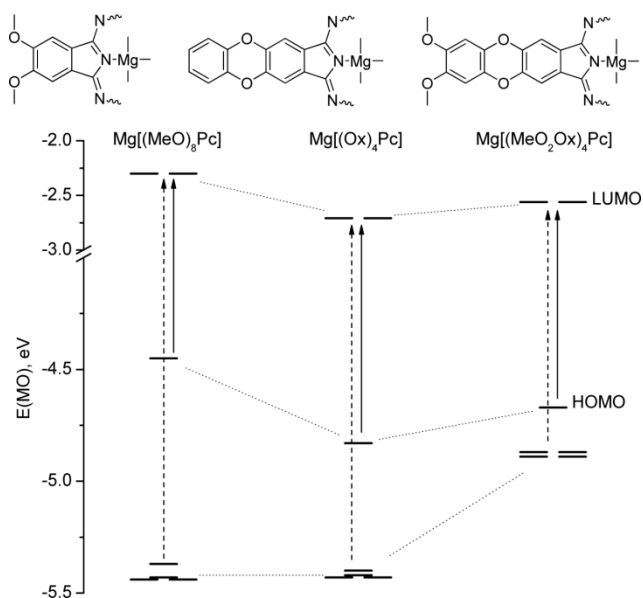


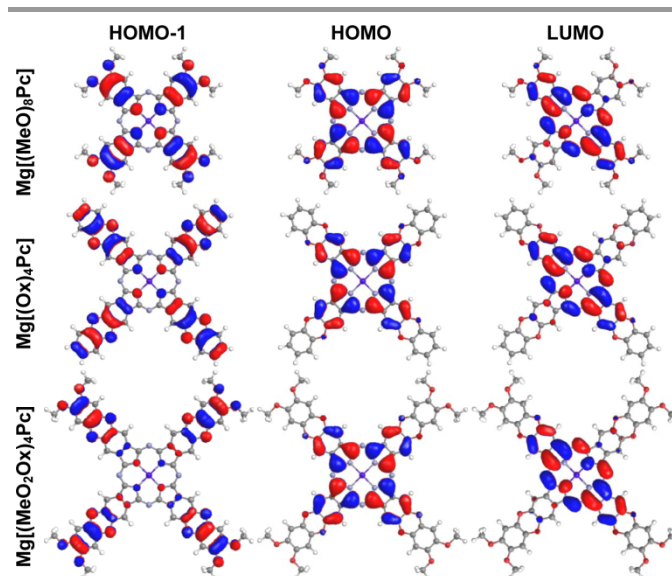
**Fig. 9.** Diagrams of frontier molecular orbitals of magnesium phthalocyanines  $\text{Mg}[(\text{MeO})_8\text{Pc}]$ ,  $\text{Mg}[(\text{Ox})_4\text{Pc}]$  and  $\text{Mg}[(\text{MeO}_2\text{Ox})_4\text{Pc}]$ . Solid arrows correspond to HOMO-LUMO transition (Q-band), dashed arrows correspond to charge transfer transitions from peripheral groups to Pc core.

Comparison of frontier orbitals in three model phthalocyanines evidences that introduction of conjugated fragments, separated by  $sp^2$ -O atom has only minor effect on HOMO-LUMO gap, therefore, strong bathochromic shift of Q-bands in this series should not be expected. So, it should be concluded that expected expansion of Pcs  $\pi$ -system was not achieved.

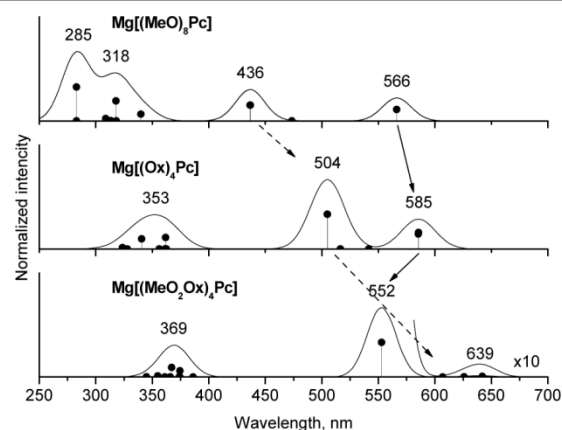
However, significant growth of energy of low-lying occupied MO's can be observed, when tetraoxybenzene fragment is introduced into Pc molecule. Analysis of 3D surfaces of calculated orbitals evidences that HOMO and LUMO do not change symmetry upon expansion of molecules. They are localized mainly on Pc core, while low-lying set of orbitals has large coefficients on peripheral substituents (Fig. 10). Therefore, transitions from these orbitals to LUMO should have charge transfer nature.

To confirm this conclusion, TDDFT prediction of UV-Vis spectra of Mg complexes was performed. Analysis of obtained results was performed with Chemissian 4.30, which can manipulate molecular orbital energy-level diagrams, calculated

and experimental UV-Vis electronic spectra, natural transition orbitals, and electronic/spin density maps. For this purpose, fragment contributions can be calculated by means of implemented tools. The data about orbitals, involved in transitions, together with arbitrary fragmentation of molecules is summarized in Table 2, and their predicted UV-Vis spectra are given in Fig. 11.



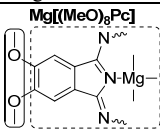
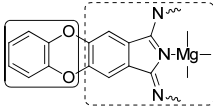
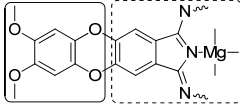
**Fig. 10.** 3D-plots of frontier MO's of model complexes  $\text{Mg}[(\text{MeO})_8\text{Pc}]$ ,  $\text{Mg}[(\text{Ox})_4\text{Pc}]$  and  $\text{Mg}[(\text{MeO}_2\text{Ox})_4\text{Pc}]$ .



**Fig. 11.** TDDFT calculated UV-Vis spectra of model complexes  $\text{Mg}[(\text{MeO})_8\text{Pc}]$ ,  $\text{Mg}[(\text{Ox})_4\text{Pc}]$  and  $\text{Mg}[(\text{MeO}_2\text{Ox})_4\text{Pc}]$ . Solid and dashed arrows indicate trends in behaviour of Q-band and CT band respectively.

In calculated spectrum of  $\text{Mg}[(\text{MeO})_8\text{Pc}]$  two major bands are observed in visible region in line with previously reported results.<sup>48,49</sup> The band at 566 nm corresponds to HOMO $\rightarrow$ LUMO transition (Q-band), while the band at 436 nm (mainly, HOMO-2 $\rightarrow$ LUMO) corresponds to CT from peripheral oxygen atoms to Pc core. However, the degree of MO localization on OMe-groups in this orbital is not very high (*ca.* 40%). Annellation of MgPc with benzo-dioxane fragment results in small red shift of the Q-band, but the CT band (mainly, HOMO-3 $\rightarrow$ LUMO) shifts by almost 70 nm. In this case, the occupied MO is localized mainly on periphery (70%).

**Table 2.** Selected lowest-excited absorption wavelengths, strengths, dominant configurations of calculated UV-Vis spectra of model complexes Mg[(MeO)<sub>8</sub>Pc], Mg[(Ox)<sub>4</sub>Pc] and Mg[(MeO<sub>2</sub>Ox)<sub>4</sub>Pc], together with contributions of molecular orbitals on donor and acceptor fragments.

Wavelength, nm (strength) assignment	Major configurations	Occupied molecular orbital		Vacant molecular orbital	
		Contribution of MO on fragment <b>D</b>	Contribution of MO on fragment <b>Pc</b>	Contribution of MO on fragment <b>D</b>	Contribution of MO on fragment <b>Pc</b>
					
<b>HOMO:</b> -4.446 eV <b>Degenerated LUMO, LUMO+1:</b> -2.301 eV <b>HOMO-LUMO gap:</b> 2.145 eV					
566 (0.436) – Q <sup>[a]</sup>	77% HOMO→LUMO 20% HOMO-2→LUMO+1	7% 39%	93% 61%	4% -/-	96% -/-
473 (0.003) – CT <sup>[b]</sup>	97% HOMO-1→LUMO	36%	64%	-/-	-/-
436 (0.596) – CT	90% HOMO-2→LUMO 7% HOMO-7→LUMO	39% 1%	61% 99%	-/- -/-	-/- -/-
					
<b>HOMO:</b> -4.828 eV <b>Degenerated LUMO, LUMO+1:</b> -2.731 eV <b>HOMO-LUMO gap:</b> 2.097 eV					
585 (0.364) – Q	62% HOMO→LUMO 36% HOMO-2→LUMO	6% 70%	94% 30%	4% -/-	96% -/-
504 (0.847) – CT	76% HOMO-2→LUMO+1 21% HOMO→LUMO	70% 6%	30% 94%	-/- -/-	-/- -/-
					
<b>HOMO:</b> -4.670 eV <b>Degenerated LUMO, LUMO+1:</b> -2.559 eV <b>HOMO-LUMO gap:</b> 2.111 eV					
642 (0.018) – CT	66% HOMO-2→LUMO+1 32% HOMO-2→LUMO	86% 86%	14% 14%	4% -/-	96% -/-
626 (0.006) – CT	90% HOMO-1→LUMO 7% HOMO-2→LUMO	84% 86%	16% 14%	-/- -/-	-/- -/-
552 (1.105) – Q	68% HOMO→LUMO 29% HOMO-2→LUMO+1	7% 86%	93% 14%	-/- -/-	-/- -/-

<sup>[a]</sup> Due to the presence of two degenerate LUMO's each of MO→LUMO transitions has a pair with the same excitation energy, but involving other LUMO. Only one of transitions is given. <sup>[b]</sup> CT – band with mainly charge-transfer contribution.

Finally, in the case of phthalocyanine, bearing tetra-oxy-benzene fragment, CT band's red shift is so strong, that this band now is found at lower-energy side of the Q-band (which itself has 29% contribution of CT configuration). Localization of involved MO's (HOMO-2 and HOMO-3) on peripheral groups is almost 90%.

To demonstrate this effect on distribution of electron density upon corresponding excitations, the maps of electron difference between the ground state and excited states for Q and CT bands were plotted (Fig. 12). Significant CT contribution to excited states of Pcs containing 15-crown-5-oxanthrene-fragments results in spectacular redistribution of electron density. We expect that synthesized herein donor-acceptor phthalocyanines find further application in optoelectronic devices.

To get preliminary insight into material chemistry of synthesized complex **8Mg** we have investigated films, prepared from its colloidal solution by AFM technique. It revealed that casting the solution onto mica surface results in formation of granular film, composed of relatively large particles with broadly dispersed height from 5 to 25 nm (Fig. 13).

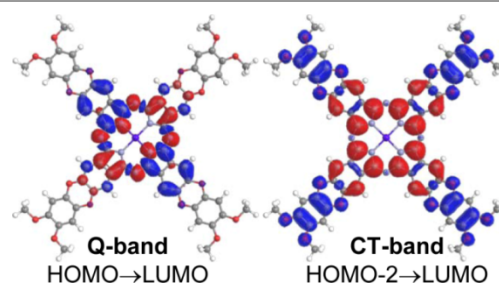


**Fig. 12.** Maps of electron difference for Mg[(MeO<sub>2</sub>Ox)<sub>4</sub>Pc], corresponding to dominant Q- and CT-band configurations. Electron density moves from blue to red area.

However, when cast film was prepared starting from dimer (**8Mg**)<sub>2</sub>(KOAc)<sub>4</sub>, formed by **8Mg** in the presence of 2 eq. KOAc, the size of particles became much smaller. In this case average height was only 5 nm and size distribution was much narrower (Fig. 14). This might be due to electrostatic repulsion of cationic supramolecules, which precludes their aggregation (as also evidenced by DLS studies of **8Mg** in the absence and in the presence of KOAc, Fig. 4). Therefore, disaggregating effect

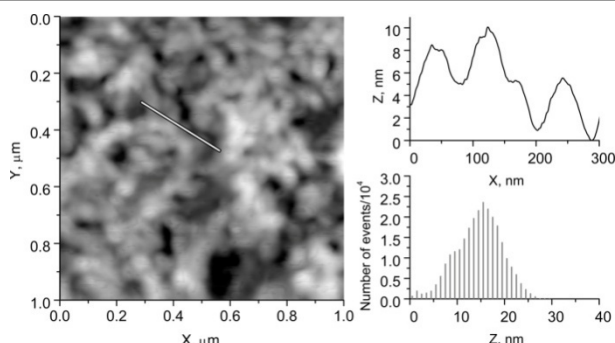


**Fig. 13.** AFM image of cast film on mica, formed by colloidal solution of **8Mg** ( $9.8 \cdot 10^{-5}$  M,  $\text{CHCl}_3$ +10 vol.% MeOH)

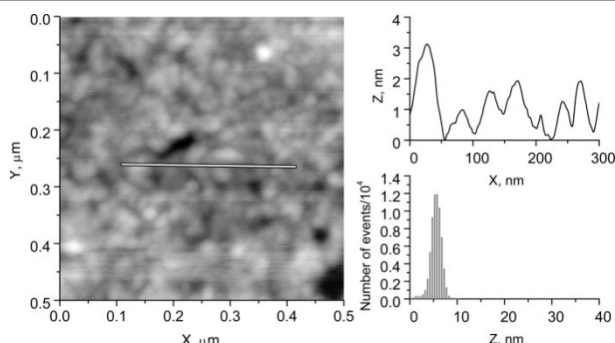


**Fig. 14.** AFM image of cast film on mica, formed by solution containing **8Mg** ( $9.8 \cdot 10^{-5}$  M) and KOAc ( $1.96 \cdot 10^{-4}$  M) in  $\text{CHCl}_3$ +10 vol.% MeOH

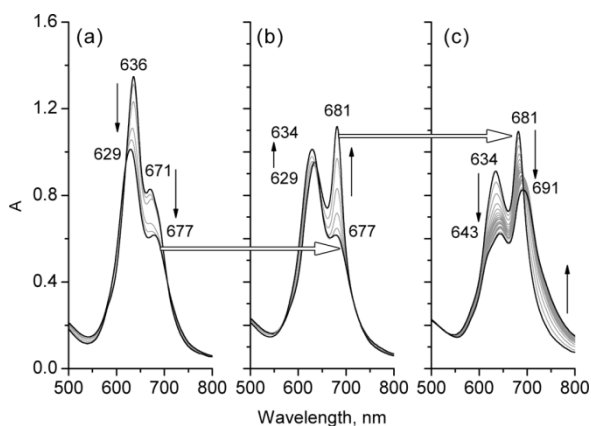


**Fig. 15.** Stepwise changes of UV-Vis spectrum of dimer  $(\mathbf{8Zn})_2(\text{KOAc})_4$  upon titration with [2.2.2]cryptand in  $\text{CHCl}_3$ +10 vol.% MeOH. (a) addition of 0→2 equiv. of cryptand; (b) addition of 2→3 equiv. of cryptand; (c) formation of nanoparticles, formed by **8Zn** during several minutes.

of potassium cations binding observed in solution, is retained in solid state and can be used to control morphology of films, formed by **8Mg**.

To get more possibilities to controlling of aggregate morphology, the reversibility of KOAc-binding was investigated on the example of less soluble complex **8Zn**. For this purpose, suspension of complex in  $\text{CHCl}_3$ +10 vol.% MeOH was treated with 2 eq. KOAc, resulting in formation of well-soluble supramolecular dimer  $(\mathbf{8Zn})_2(\text{KOAc})_4$ . Then, the aliquot of the obtained solution was titrated with solution of [2.2.2]cryptand – well-known ligand, forming very stable

complexes with  $\text{K}^+$  ions.<sup>50</sup> Upon titration, changes in UV-Vis spectra were observed, evidencing of stepwise destruction of supramolecular dimer. Each of steps was characterized by its own set of isobestic points. Transformations of Q-band region is given in Fig. 15. At first step simultaneous decrease of Q- and CT-bands was observed with hypso- and bathochromic shifts respectively. Then, the band at 677 nm (assigned to CT-band in dimer) started to grow. Resulting solution became unstable and turbidness appeared within several minutes. At this step, UV-Vis spectrum of solution started its own evolution – both bands shifted to the red and absorption in NIR region also gained intensity, suggesting that J-aggregate with brickwork-like architecture could be formed.

Previous studies of dimerization of crown-Pcs, induced by interaction with potassium salts, reveal non-linear cooperativity of this process – binding of first cation by two receptor molecules results in formation of pivot-joint dimer.<sup>51,52</sup> This dimer is already pre-organized for second cation binding, which leads to the formation of rigid eclipsed dimer. Further binding of third and fourth cations doesn't lead to changes in dimer architecture.<sup>14,53</sup>

Similar behaviour can be expected in the case of reverse process – upon interaction of dimer  $(\mathbf{8Zn})_2(\text{KOAc})_4$  with cryptand. Removal of first two cations from dimer, should not lead to loss of cofacial arrangement of Pc molecules within dimer. This can correspond to the first step, when the general appearance of UV-Vis spectra does not change (Fig. 15a). Then, removal of third cation can lead to formation of pivot-joint dimer, which results in further changes in UV-Vis (Fig. 15b). Simultaneously, removal of cations decreases effect of electrostatic repulsion between positively charged dimeric species and at some step aggregation becomes more favourable (Fig. 15c).

At this step, the sample of solution was cast on mica and studied by AFM. It evidenced of formation of well-defined nanoparticles with average diameter  $\sim 20$  nm and height  $\sim 1$  nm (Fig. 16). Further storage of solution results in coagulation of nanoparticles with the formation of dark-green precipitate. More detailed studies will be performed to study organization of molecules of synthesized Pcs within nanoparticles.

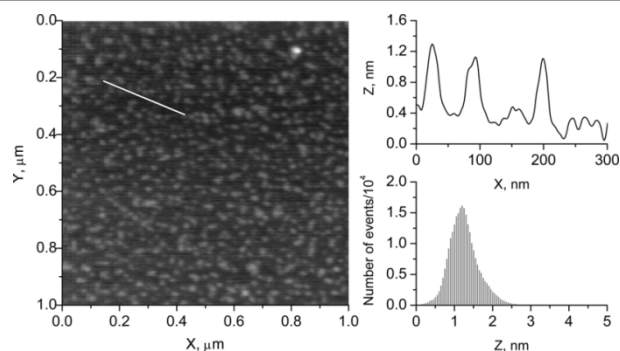


**Fig. 16.** AFM image of nanoparticles, formed by **8Zn** upon titration of  $(\mathbf{8Zn})_2(\text{KOAc})_4$  with [2.2.2]cryptand.

## Conclusions

In the present manuscript we describe efficient synthesis of phthalocyanines bearing lateral 15-crown-5-oxanthrene units, conjugated with tetrapyrrolic core.

The obtained compound turned out to be very difficult to characterize due to formation of insoluble aggregates. However, interaction with potassium ions afforded formation of soluble well-defined supramolecular dimers, which could be studied by numerous physical-chemical techniques. Potassium cations can be reversibly removed by [2.2.2]cryptand, resulting in formation of monodisperse nanoparticles.

Design of such systems was based on assumption that conjugation of electron-rich tetra-oxy-benzene units with Pc core through bridging  $sp^2$ -O atoms would result in expansion of Pcs aromatic system, which in turn would lead to Q-bands shift to near-IR region. However, comparative studies of newly synthesized complexes with "classical" crown-phthalocyanines by means of UV-Vis studies together with TDDFT calculations did not confirm anticipated expansion of  $\pi$ -system – neither bathochromic shift of the Q-band, nor HOMO-LUMO gap contraction were observed. However, calculations revealed spectacular redistribution of electronic density upon photoexcitation of synthesized complexes, which results in appearance of the new charge-transfer band in near-IR, absent in UV-Vis spectra of "classical" crown-phthalocyanines. Therefore, the goal to improve light-harvesting properties of phthalocyanines in near-IR was finally achieved not by means of expansion of aromatic system, but by arrangement of conditions for efficient charge transfer from peripheral electron-donating groups to Pc acceptor.

Absorption of nanosized aggregates, formed by synthesized complexes, cover region up to 900 nm. Therefore, the synthesized complexes can be referred to panchromatic photosensitizers with controllable solubility, which can find applications in optoelectronic devices.

## Acknowledgements

Design and synthesis of complexes was performed within the project, supported by grants from Council under the President of the Russian Federation for State Support of Young Scientists and Leading Scientific Schools (MK-1606.2013.3) and Russian Scientific Foundation (14-13-01373). Quantum-chemical modeling was performed within the project, supported by grant from Russian Foundation for Basic Research (14-03-31639-mol\_a). AFM studies were supported by grant from OPTEC company (Contract № 49/2014/75-Msk). The authors are grateful to Dr. G.A. Kirakosyan and Dr. K.P. Birin for NMR measurements, to Dr. I.P. Stolyarov for elemental analysis, to Dr. L.I. Demina for measurements of IR-spectra, to Dr. V.V. Visotskii for DLS measurements.

## Experimental Section

### General considerations

Benzo-15-crown-5 **1**,  $\text{POCl}_3$ , N-methylformanilide,  $\text{KH}_2\text{PO}_4$ , 10% Pd/C, 4,5-dichlorophthalonitrile **6**, N-bromosuccinimide (NBS),  $\text{Zn}(\text{CN})_2$ , dipalladium tris(dibenzalacetone)  $\text{Pd}_2(\text{dba})_3$ , 1,1'-diphenylphosphinoferrocene (dppf), 1,8-diazabicyclo[5.4.0]undecene-7 (DBU), [2.2.2]cryptand,  $\text{Zn}(\text{OAc})_2$ ,  $\text{Mg}(\text{OAc})_2$  and solvents - isoamyl alcohol (*i*-AmOH), *o*-dichlorobenzene (*o*-DCIB), DMF, DMAA were available from commercial suppliers (Acros, Merck, Aldrich, Sigma). *i*-AmOH was distilled over sodium under argon. DBU and *o*-DCIB were dried and distilled over  $\text{CaH}_2$  under reduced pressure and stored under argon. Neutral alumina (Merck) and silica (Macherey Nagel, Kieselgel 60) were used for column chromatography. Chloroform (CHIMMED, stabilized with 0.6-1%EtOH) was dried over  $\text{CaCl}_2$  and distilled over  $\text{CaH}_2$ . Fremy's salt (potassium nitrosodisulphonate,  $(\text{KOSO}_2)_2\text{NO}$ ) was synthesized by previously reported method.<sup>33</sup> NMR spectra were recorded with a Bruker Avance 600 spectrometer. NMR spectra were referenced against the residual solvent signal.<sup>54</sup> UV-Vis spectra were measured with a Varian Cary-100 spectrometer in quartz cells with 1 cm optical path. Spectrophotometric titrations were performed in 1cm quartz cells with Teflon stopper. Dosage of titrant was performed with syringe pump LA-100 (Landgraf HLL). FT-IR Nexus (Nicolet) spectrometer with micro-ATR accessory (Pike) was used to record IR spectra. Elemental analysis was performed with a Carlo-Erba 1106 instrument. MALDI TOF mass-spectra were measured on Ultraflex spectrometer (Bruker Daltonics) with 2,5-dihydroxybenzoic acid (DHB), used as a matrix. DLS measurements were performed on Zsizer instrument (Malvern).

### Aldehyde **2**

$\text{POCl}_3$  (13.7 ml, 0.150 mol) was added to N-methylformanilide (18.4 ml, 0.150 mol) and mixture was stirred for 15 min until solidification. Benzo-15-crown-5 **1** (20.0 g, 0.075 mol) was added to obtained solid and mixture was heated to 75 °C for 3 h resulting in formation of dark orange viscous melt. After cooling to room temperature, aqueous HCl (200 ml of water and 100 ml of conc. HCl) was added and mixture was extracted with  $\text{CHCl}_3$  (4x100ml), organic extracts were washed with water, dried over  $\text{CaCl}_2$ , and the solvent was removed under reduced pressure. Resulting oil was mixed with cold *i*-PrOH, the mixture was cooled to -20°C to cause crystallization and filtered. Obtained crystals were washed with cold *i*-PrOH and dried under reduced pressure yielding **2** as white powder (16.3 g, 74%). NMR data is in accordance with the previously reported.<sup>55</sup>  $^1\text{H}$  NMR (600 MHz,  $\text{CDCl}_3$ )  $\delta$  ppm: 9.82 (s, 1H, COH), 7.42 (dd,  $J = 8.2, 1.8$  Hz, 1H, 5- $\text{H}_{\text{Ar}}$ ), 7.37 (d,  $J = 1.8$  Hz, 1H, 3- $\text{H}_{\text{Ar}}$ ), 6.93 (d,  $J = 8.2$  Hz, 1H, 6- $\text{H}_{\text{Ar}}$ ), 4.23 – 4.14 (m, 4H,  $\alpha, \alpha'$ - $\text{OCH}_2$ ), 3.95 – 3.88 (m, 4H,  $\beta, \beta'$ - $\text{OCH}_2$ ), 3.80 – 3.72 (m, 8H,  $\gamma, \delta, \gamma', \delta'$ - $\text{OCH}_2$ ).  $^{13}\text{C}$  NMR (151 MHz,  $\text{CDCl}_3$ )  $\delta$  ppm:

190.95, 154.76, 149.57, 130.38, 126.97, 112.15, 111.49, 71.38, 70.51, 70.44, 69.42, 69.32, 68.97, 68.87.

### Phenol 3

4'-formylbenzo-15-crown-5 **2** (5.0 g, 0.017 mol) was dissolved in 60 ml CHCl<sub>3</sub>. The solution of 30% H<sub>2</sub>O<sub>2</sub> (3.5 ml, 0.034 mol) and conc. H<sub>2</sub>SO<sub>4</sub> (0.4 ml) in methanol (60 ml) was added dropwise during 1.5 hours. Then the mixture was stirred at room temperature for 12 hours. Water (60 ml) was added and the mixture was extracted with CHCl<sub>3</sub> (4x50 ml). Organic extracts were washed with water, dried over CaCl<sub>2</sub>, and the solvent was removed under reduced pressure. The product was purified by using chromatography on Al<sub>2</sub>O<sub>3</sub> (elution with CHCl<sub>3</sub>/CH<sub>3</sub>OH, 9:1 vol.) yielding **3** as pink oil, which slowly solidified (3.78 g, 79%). NMR data is in accordance with the previously reported.<sup>56</sup> <sup>1</sup>H NMR (600 MHz, CDCl<sub>3</sub>) δ ppm: 6.70 (d, *J* = 8.6 Hz, 1H, 6-H<sub>Ar</sub>), 6.39 (d, *J* = 2.8 Hz, 1H, 3-H<sub>Ar</sub>), 6.31 (dd, *J* = 8.6, 2.8 Hz, 1H, 5-H<sub>Ar</sub>), 5.79 (s, 1H, OH), 4.08 – 4.01 (m, 4H, α,α'-OCH<sub>2</sub>), 3.89 – 3.84 (m, 4H, β,β'-OCH<sub>2</sub>), 3.77 – 3.72 (m, 8H, γ,δ,γ',δ'-OCH<sub>2</sub>). <sup>13</sup>C NMR (151 MHz, CDCl<sub>3</sub>) δ ppm: 151.26, 150.52, 142.90, 116.81, 106.97, 102.61, 71.09, 70.99, 70.89, 70.73, 70.58, 70.05, 69.66, 68.69.

### Quinone 4

Solution of KH<sub>2</sub>PO<sub>4</sub> (1.18 g, 8.68 mmol) in 30 ml of water was cooled down on an ice bath. Solution of freshly prepared (KOSO<sub>2</sub>)<sub>2</sub>NO (1.75 g, 6.53 mmol) in 60 ml of water and solution of 4'-hydroxybenzo-15-crown-5 (1.48 g, 5.21 mmol) in 7.5 ml of methanol were added. The mixture was stirred for 1.5h at 0 °C. The resulting precipitate was filtered, washed with water and discarded. Combined filtrates were extracted with CHCl<sub>3</sub> (4x50 ml), dried over Na<sub>2</sub>SO<sub>4</sub> and the solvent was removed in reduced pressure. The product was purified by using chromatography on silica (elution with CHCl<sub>3</sub>/CH<sub>3</sub>OH, 98:2 vol.) yielding **4** as orange powder (0.89 g, 57%). Storage of **4** at room temperature results in its slow decomposition over several days, however it is stable when kept in the freezer at -15 °C. M.p. 153°C. <sup>1</sup>H NMR (600 MHz, CDCl<sub>3</sub>) δ ppm: 5.69 (s, 1H, -CH=), 4.14 – 4.02 (m, 2H, α-OCH<sub>2</sub>), 3.93 – 3.83 (m, 2H, β-CH<sub>2</sub>), 3.72 (m, 4H, γ,δ-OCH<sub>2</sub>). <sup>13</sup>C NMR (151 MHz, CDCl<sub>3</sub>) δ ppm: 179.09, 163.26, 103.25, 71.04, 69.87, 69.32, 68.00. FT-IR (ν, cm<sup>-1</sup>): 3068, 2944, 2860, 1646, 1578, 1428, 1400, 1374, 1354, 1302, 1248, 1174, 1132, 1093, 1073, 1030, 982, 933, 916, 892, 853, 822, 752. Anal. calc. for C<sub>14</sub>H<sub>18</sub>O<sub>7</sub>: C 56.37, H 6.08; found: C 56.49, H 6.21.

### Phthalonitrile 7

Mixture of quinone **4** (0.26 g, 0.87 mmol) and 10% Pd/C (13 mg) in DMF (15 ml) was degassed and then stirred 2 hours in a stream of H<sub>2</sub> until it became colorless, which corresponded to formation of catechol **5**. Then the mixture was taken into a syringe through nylon syringe filter and resulting colourless filtrate was transferred into a flask with degassed mixture of 4,5-dichlorophthalonitrile **6** (0.17 g, 0.86 mmol) and K<sub>2</sub>CO<sub>3</sub> (0.36 g, 2.61 mmol). Resulted suspension was stirred for 18 hours at 70°C. Then it was poured into water, precipitate was

filtered, washed with water and dried in vacuum. The product was stirred under reflux in ethanol, and then solid was filtered and dried yielding 0.235 g of **7** as yellow powder. EtOH washings were evaporated to dryness. The resulted oil was purified by using chromatography on silica (elution with CHCl<sub>3</sub>/CH<sub>3</sub>OH, 9:1) yielding additionally 0.065 g of **7**. Overall yield of **7** was 300 mg, 81%. M.p. 231°C. <sup>1</sup>H NMR (600 MHz, CDCl<sub>3</sub>) δ ppm: 7.14 (s, 1H, 6,9-H<sub>Ar</sub>), 6.47 (s, 1H, 1,4-H<sub>Ar</sub>), 4.10 – 4.04 (m, 2H, α-CH<sub>2</sub>), 3.92 – 3.86 (m, 2H, β-CH<sub>2</sub>), 3.78 – 3.71 (m, 4H, γ,δ-CH<sub>2</sub>). <sup>13</sup>C NMR (151 MHz, CDCl<sub>3</sub>) δ ppm: 146.57, 146.19, 133.79, 121.43, 114.82, 111.62, 103.93, 71.13, 70.62, 70.01, 69.52. FT-IR (ν, cm<sup>-1</sup>): 3034, 2945, 2866, 2231 (ν<sup>C=N</sup>), 1594, 1566, 1517, 1500, 1456, 1447, 1435, 1381, 1371, 1305, 1269, 1232, 1190, 1176, 1126, 1093, 1059, 1042, 1011, 975, 948, 928, 897, 869, 857, 829, 816. Anal. calcd for C<sub>22</sub>H<sub>20</sub>N<sub>2</sub>O<sub>7</sub>: C 62.26, H 4.75, N 6.60; found: C 62.13, H 4.48, N 6.70

### Zinc phthalocyaninate 8Zn

The mixture of nitrile **7** (42.4 mg, 0.1 mmol), Zn(OAc)<sub>2</sub> (9.2 mg, 0.05 mmol) and DBU (15 μl, 0.1 mmol) in 1 ml of isoamyl alcohol was refluxed for 15 h under slow stream of Ar. After cooling reaction mixture was added dropwise to hexane (50 ml). The reaction mixture was filtered through a membrane filter. The obtained precipitate was washed with ethanol. Then the membrane with the solid was moistened with ethanol, folded, placed into a Soxhlet glass thimble with sintered bottom and extracted with ethanol for 1 d. The yellowish extract was discarded and the solid phthalocyanine remaining in the thimble was peeled off the membrane under sonication in chloroform, the solvent was evaporated, and a dark powder of **8Zn** was dried in vacuum. Yield – 25 mg, 57%. MALDI TOF: calcd for C<sub>88</sub>H<sub>80</sub>ZnN<sub>8</sub>O<sub>28</sub>: 1760.4, found: 1760.3. FT-IR (ν, cm<sup>-1</sup>): 2909, 2863, 1717, 1606, 1588, 1518, 1491, 1461, 1401, 1343, 1232, 1202, 1184, 1136, 1086, 1020, 988, 947, 897, 872, 851, 763, 741, 725. Stock solution for UV-Vis spectroscopy and AFM measurements was obtained by dissolution of **8Zn** (7.6 mg, ) and KOAc (0.8 mg) in mixture of 45 ml CHCl<sub>3</sub> and 5 ml MeOH under sonication. UV-Vis of resulting (**8Zn**)<sub>2</sub>(KOAc)<sub>4</sub>: λ, nm (A<sub>rel</sub>) 309 (0.93), 350 (0.97), 445 (0.20), 636 (1.00), 670 (0.61).

### Magnesium phthalocyaninate 8Mg

The mixture of nitrile **7** (100 mg, 0.236 mmol), Mg(OAc)<sub>2</sub> (21 mg, 0.118 mmol) and DBU (35 μl, 0.236 mmol) in 5 ml of isoamyl alcohol was refluxed under a slow stream of Ar for 15 h. Then solvent was removed in vacuo and resulting dark residue was sonicated with 50% aq. EtOH, precipitate was filtered, washed with aq. EtOH, followed by EtOH until washings were colourless. Resulting dark-green powder was washed off the filter with CHCl<sub>3</sub>/MeOH mixture. Evaporation of solvent afforded **8Mg** as dark green solid (83 mg, 81%). MALDI TOF: calcd for C<sub>88</sub>H<sub>81</sub>MgN<sub>8</sub>O<sub>28</sub>: 1722.50; found: 1722.90. FT-IR (ν, cm<sup>-1</sup>): 2861, 1604, 1586, 1507, 1453, 1394, 1265, 1233, 1176, 1129, 1077, 1017, 942, 887, 749, 738, 726. Stock solution for UV-Vis and AFM measurements was prepared by dissolving of **8Mg** (8.4 mg) in mixture of 45 ml

CHCl<sub>3</sub> and 5 ml MeOH. UV-Vis (CHCl<sub>3</sub> + 10% MeOH)  $\lambda$ , nm (lg $\epsilon$ ): 686 (4.78), 636 (4.63), 439 (4.00), 355 (4.79), 310 (4.76). Sample of supramolecular dimer for NMR measurements was prepared by dissolving of **8Mg** in CDCl<sub>3</sub>/CD<sub>3</sub>OD (4:1 vol.) in the presence of few crystals of K<sub>2</sub>CO<sub>3</sub>. <sup>1</sup>H-NMR (600 MHz, CDCl<sub>3</sub>/CD<sub>3</sub>OD)  $\delta$  ppm.: 7.14 (s, 2H, CH<sub>Ar</sub>), 6.48 (s, 2H, CH<sub>Ar</sub>), 4.07-4.09 (m, 4H,  $\alpha$ -CH<sub>2</sub>), 3.88-3.90 (m, 4H,  $\beta$ -CH<sub>2</sub>), 3.71-3.75 (m, 8H,  $\gamma,\delta$ -CH<sub>2</sub>). UV-Vis spectrum of resulting dimer –  $\lambda$ , nm (A<sub>rel</sub>) 307 (0.76), 353 (1.00), 437 (0.18), 636 (0.92), 671 (0.56).

#### Dibromide **9**

Benzo-15-crown-5 **1** (21 g, 78.3 mmol) was dissolved in 225 ml of dry CHCl<sub>3</sub>, NBS (30 g, 0.168 mol) was added and reaction mixture was refluxed for 4 h. Reaction mixture was cooled in the freezer, precipitate of succinimide was filtered off, filtrate was partially evaporated and cooled once again to remove more succinimide by filtration. Residual filtrate was evaporated to dryness and recrystallized from EtOH, affording dibromobenzo-15-crown-5 **9** as white plates. Yield – 25.4 g, 80%. NMR data is in accordance with the previously reported.<sup>13,57</sup> <sup>1</sup>H NMR (600 MHz, CDCl<sub>3</sub>)  $\delta$ , ppm: 7.07 (s, 2H, H<sub>Ar</sub>); 4.09 (m, 4H,  $\alpha$ -CH<sub>2</sub>); 3.88 (m, 4H,  $\beta$ -CH<sub>2</sub>), 3.73 (s, 8H,  $\gamma,\delta$ -CH<sub>2</sub>). <sup>13</sup>C NMR (151 MHz, CDCl<sub>3</sub>)  $\delta$  ppm: 149.21, 118.63, 115.34, 71.24, 70.54, 69.51, 69.40.

#### Phthalonitrile **10**

Dibromide **9** (1.64 g, 3.85 mmol) was mixed with Zn(CN)<sub>2</sub> (678 mg, 5.77 mmol), Pd<sub>2</sub>(dba)<sub>3</sub> (60 mg, 0.11 mmol) and dppf (70 mg, 74  $\mu$ mol). Solids were flushed with Ar and 5 ml of dry DMAA was added. Mixture was heated to 120 °C and stirred under Ar for 2.5 h. After cooling, it was filtered through the layer of silica, solids were washed with EtOAc and combined filtrates were evaporated to dryness. After column chromatography on silica with gradient elution with CHCl<sub>3</sub>/MeOH mixture, target phthalonitrile **10** was obtained as white solid. Yield – 1.00 g (81%). NMR data is in accordance with the previously reported<sup>13,57</sup>. <sup>1</sup>H NMR (600 MHz, CDCl<sub>3</sub>)  $\delta$ , ppm: 7.11 (s, 2H, H<sub>Ar</sub>), 4.20 (m, 4H,  $\alpha$ -CH<sub>2</sub>), 3.92 (m, 4H,  $\beta$ -CH<sub>2</sub>), 3.75 and 3.71 (2m, 2x8H,  $\gamma,\delta$ -CH<sub>2</sub>). <sup>13</sup>C NMR (151 MHz, CDCl<sub>3</sub>)  $\delta$  ppm: 152.66, 116.39, 115.88, 108.99, 71.25, 70.24, 69.33, 68.83.

#### Magnesium tetra-15-crown-5-phthalocyaninate **11Mg**

The mixture of dicyano-benzo-15-crown-5 **9** (64 mg, 0.2 mmol) with Mg(OAc)<sub>2</sub> (18 mg, 0.1 mmol) and DBU (30  $\mu$ l, 0.2 mmol) was refluxed for 1 day under slow stream of Ar. After cooling, reaction mixture was added dropwise to hexane and resulting precipitate was filtered and washed off the filter with CHCl<sub>3</sub>. Chromatography on alumina in CHCl<sub>3</sub>/MeOH mixture afforded dark green complex **11Mg**, which was additionally purified by Bio-Beads SX-1 column packed in CHCl<sub>3</sub>+5vol.%MeOH. Yield – 39.6 mg (61%). MALDI TOF: calcd for C<sub>64</sub>H<sub>72</sub>MgN<sub>8</sub>O<sub>20</sub>: 1296.5; found: 1269.6. UV-Vis (CHCl<sub>3</sub> + 10% MeOH)  $\lambda$ , nm (lg $\epsilon$ ): 680 (5.26), 614 (4.51), 360 (5.01), 293 (4.66). <sup>1</sup>H NMR (300 MHz, DMSO, 90 °C)  $\delta$ , ppm: 8.95 (s,

8H, H<sub>Ar</sub>), 4.71 (m, 16H,  $\alpha$ -CH<sub>2</sub>), 4.10 (m, 16H,  $\beta$ -CH<sub>2</sub>), 3.85 and 3.89 (2m, 2x16H,  $\gamma,\delta$ -CH<sub>2</sub>).

#### X-ray diffraction studies

Yellow single prismatic crystals of phthalonitrile **7** were obtained by slow evaporation of its solution in CH<sub>2</sub>Cl<sub>2</sub>:CH<sub>3</sub>OH (10:1 vol.) mixture. Single-crystal X-ray diffraction experiments were carried out on Bruker SMART APEX II diffractometer with a CCD area detector (graphite monochromator, Mo-K $\alpha$  radiation,  $\lambda$  = 0.71073 Å,  $\omega$ -scans). a = 7.7428(14) Å, b = 12.863(2) Å, c = 20.288(4) Å,  $\beta$  = 92.172(3)°, V=2019.1(6) Å<sup>3</sup> (150K), Z = 4, D<sub>calc</sub> = 1.396 g/cm<sup>3</sup>, 21428 measured reflections, 5285 [R(int) = 0.0307] independent reflections with F<sup>2</sup> > 2 $\sigma$ (I),  $\mu$  = 0.105 cm<sup>-1</sup>, R<sub>1</sub> = 0.0475, wR<sub>2</sub> = 0.1359. The semi-empirical method SADABS<sup>58</sup> was applied for the absorption correction. The structures were solved by direct methods and refined by the full-matrix least-squares technique against F<sup>2</sup> with the anisotropic displacement parameters for all non-hydrogen atoms. All the hydrogen atoms in the complexes were placed geometrically and included in the structure factors calculation in the riding motion approximation. All the data reduction and further calculations were performed using the SAINT<sup>59</sup> and SHELXTL-97<sup>60</sup> program packages. CCDC-1014940 contains the supplementary crystallographic data for this paper.

#### Computational details

Geometry optimization was performed without any symmetry constraints using “AccOpt” preset, implemented in ORCA 2.9.1 software.<sup>45</sup> It utilizes BP86 functional, TZV(p) and TZV(2d) basis sets for H atoms and other main group atoms respectively<sup>61,62</sup> with tight SCF convergence criteria. TDDFT calculations were performed for the obtained DFT optimized structures at B3LYP/6-31G(d) level.<sup>63-65</sup> 32 vertical excitations were calculated with RIJCOSX approximation, which affords significant speedup for calculations of large molecules.<sup>66</sup> The Ahlrichs auxiliary basis sets<sup>67,68</sup> for RI approximation and Ahlrichs polarization functions were obtained from the TurboMole basis set library. Computer program Chemissian 4.30 (by L. Skripnikov) was used to analyze and visualize quantum-chemical calculations. For the current version see www.chemissian.com.

#### Atomic force microscopy measurements

Samples for AFM were prepared by casting of 5  $\mu$ l of 10<sup>-4</sup> M solutions in CHCl<sub>3</sub>/MeOH (9:1 vol.) onto freshly peeled mica surface. The AFM investigation was carried with AFM model Enviroscope and controller Nanoscope V from Bruker. Image acquisition was performed in tapping mode. Silicon cantilevers NSG10 (resonance frequency 250 kHz, force constant 15 Nm<sup>-1</sup>, curvature radius 10 nm) from NT-MDT Corporation (Russia) were used. Data were processed by software WSxM 5.0 Develop 6.5 Nanotec Electronica (Spain, Madrid).<sup>69</sup>

## Notes and references

<sup>a</sup> A.N. Frumkin Institute of Physical Chemistry and Electrochemistry, Russian Academy of Sciences, 119071, Leninskiy pr., 31, bldg.4, Moscow, Russia, E-mail: *Martynov.Alexandre@gmail.com*

<sup>b</sup> N.S. Kurnakov Institute of General and Inorganic Chemistry, Russian Academy of Sciences, 119991, Leninskiy pr., 31, Moscow, Russia, E-mail: *yulia@igic.ras.ru*

† Electronic supplementary information (ESI) available: <sup>1</sup>H NMR, <sup>13</sup>C NMR spectral data (Figs. S1-S4) and optimized Cartesian coordinates (Tables S1-S3). See DOI: 10.1039/b000000x/

- J. Mack, Y. Asano, N. Kobayashi, and M. J. Stillman, *J. Am. Chem. Soc.*, 2005, **127**, 17697–711.
- J. Mack and N. Kobayashi, *Chem. Rev.*, 2011, **111**, 281–321.
- T. Nyokong, in *Functional Phthalocyanine Molecular Materials*, ed. J. Jiang, Springer Berlin Heidelberg, Berlin, Heidelberg, 2010, vol. 135, pp. 45–87.
- A. W. Snow, in *The Porphyrin Handbook*, eds. K. M. Kadish, K. M. Smith, and R. Guilard, Academic Press, New York, 2003, vol. 17, pp. 129–176.
- S. Dhami and D. Phillips, *J. Photochem. Photobiol. A Chem.*, 1996, **100**, 77–84.
- N. R. S. Gobo, T. J. Brocksom, J. Zukerman-Schpector, and K. T. de Oliveira, *European J. Org. Chem.*, 2013, **2013**, 5028–5031.
- N. B. McKeown, S. Makhseed, K. J. Msayib, L.-L. Ooi, M. Helliwell, and J. E. Warren, *Angew. Chem. Int. Ed.*, 2005, **44**, 7546–7549.
- Y. Zhang, X. Cai, Y. Bian, and J. Jiang, in *Functional Phthalocyanine Molecular Materials*, ed. J. Jiang, Springer Berlin Heidelberg, Berlin, Heidelberg, 2010, vol. 135, pp. 275–322.
- Y. G. Gorbunova, A. G. Martynov, and A. Y. Tsivadze, in *Handbook of Porphyrin Science*, eds. K. M. Kadish, K. M. Smith, and R. Guilard, World Scientific Publishing, 2012, vol. 24, pp. 271–388.
- A. Y. Tsivadze, *Russ. Chem. Rev.*, 2004, **73**, 5–23.
- Y. G. Gorbunova, L. A. Lapkina, and A. Y. Tsivadze, *J. Coord. Chem.*, 2003, **56**, 1223–1232.
- Y. G. Gorbunova, L. A. Lapkina, A. G. Martynov, I. V. Biryukova, and A. Y. Tsivadze, *Russ. J. Coord. Chem.*, 2004, **30**, 245–251.
- V. Ahsen, E. Yilmazer, M. Ertaş, and Ö. Bekâröglü, *J. Chem. Soc., Dalton Trans.*, 1988, 401–406.
- N. Kobayashi and A. B. P. Lever, *J. Am. Chem. Soc.*, 1987, **109**, 7433–7441.
- O. E. Sielcken, M. M. Van Tilborg, M. F. M. Roks, R. Hendriks, W. Drenth, and R. J. M. Nolte, *J. Am. Chem. Soc.*, 1987, **109**, 4261–4265.
- F. D'Souza, E. Maligaspe, K. Ohkubo, M. E. Zandler, N. K. Subbaiyan, and S. Fukuzumi, *J. Am. Chem. Soc.*, 2009, **131**, 8787–8797.
- A. G. Martynov, Y. G. Gorbunova, and A. Y. Tsivadze, *Prot. Met.*, 2011, **47**, 465–470.
- H. Engelkamp, S. Middelbeek, and R. J. M. Nolte, *Science*, 1999, **284**, 785–788.
- J. Sly, P. Kasák, E. Gomar-Nadal, C. Rovira, L. Górriz, P. Thordarson, D. B. Amabilino, A. E. Rowan, and R. J. M. Nolte, *Chem. Commun.*, 2005, 1255–1257.
- L. Wu, Q. Wang, J. Lu, Y. Bian, J. Jiang, and X. Zhang, *Langmuir*, 2010, **26**, 7489–7497.
- A. D. Grishina, F. Y. Konnov, Y. G. Gorbunova, Y. Y. Enakieva, L. Y. Pereshivko, T. V. Krivenko, V. Savelyev, A. V. Vannikov, and A. Y. Tsivadze, *Russ. J. Phys. Chem. A*, 2007, **81**, 982–989.
- A. D. Grishina, Y. G. Gorbunova, L. Y. Pereshivko, A. A. Nekrasov, Y. Y. Enakieva, T. V. Krivenko, V. Savelyev, A. V. Vannikov, and A. Y. Tsivadze, *Prot. Met.*, 2009, **45**, 535–542.
- A. D. Grishina, Y. G. Gorbunova, Y. Y. Enakieva, T. V. Krivenko, V. Savelyev, A. V. Vannikov, and A. Y. Tsivadze, *High Energy Chem.*, 2008, **42**, 297–304.
- A. V. Vannikov, A. D. Grishina, Y. G. Gorbunova, A. A. Isakova, T. V. Krivenko, V. I. Zolotarevskii, L. A. Lapkina, V. V. Savel'ev, and A. Y. Tsivadze, *High Energy Chem.*, 2014, **48**, 97–103.
- Y. Y. Enakieva, Y. G. Gorbunova, S. E. Nefedov, and A. Y. Tsivadze, *Mendeleev Commun.*, 2004, **14**, 193–194.
- A. G. Martynov, O. V. Zubareva, Y. G. Gorbunova, S. G. Sakharov, S. E. Nefedov, F. M. Dolgushin, and A. Y. Tsivadze, *Eur. J. Inorg. Chem.*, 2007, 4800–4807.
- A. D. Grishina, Y. G. Gorbunova, V. I. Zolotarevskiy, L. Y. Pereshivko, Y. Y. Enakieva, T. V. Krivenko, V. Savelyev, A. V. Vannikov, and A. Y. Tsivadze, *J. Porphyrins Phthalocyanines*, 2009, **13**, 92–98.
- I. Goldberg and U. Shmueli, *Acta Crystallogr. Sect. B Struct. Crystallogr. Cryst. Chem.*, 1973, **29**, 432–440.
- J. Hellberg, E. Dahlstedt, and M. E. Pelcman, *Tetrahedron*, 2004, **60**, 8899–8912.
- K. Msayib, S. Makhseed, and N. B. McKeown, *J. Mater. Chem.*, 2001, 2784–2789.
- N. B. McKeown, S. Makhseed, and P. M. Budd, *Chem. Commun.*, 2002, **44**, 2780–1.
- B. A. Kamino and T. P. Bender, *Dalt. Trans.*, 2013, **42**, 13145–50.
- H. Zimmer, D. C. Lankin, and S. W. Horgan, *Chem. Rev.*, 1971, **408**, 1968–1970.
- P. Singh and J. D. McKinney, *Acta Crystallogr. Sect. B Struct. Crystallogr. Cryst. Chem.*, 1978, **34**, 2956–2957.
- Z. Iqbal, A. Lyubimtsev, and M. Hanack, *Synlett*, 2008, 2287–2290.
- A. G. Martynov, K. P. Birin, Y. G. Gorbunova, and A. Y. Tsivadze, *Macroheterocycles*, 2013, **6**, 23–32.
- A. G. Martynov, Y. G. Gorbunova, S. E. Nefedov, A. Y. Tsivadze, and J.-P. Sauvage, *Eur. J. Org. Chem.*, 2012, **2012**, 6888–6894.
- L. A. Lapkina, Y. G. Y. G. Gorbunova, D. O. Gil, V. K. Ivanov, N. Y. Konstantinov, and A. Y. Tsivadze, *J. Porphyr. Phthalocyanines*, 2013, **17**, 564–572.
- A. G. Martynov and Y. G. Gorbunova, *Inorg. Chim. Acta*, 2007, **360**, 122–130.
- A. G. Martynov and Y. G. Gorbunova, *Polyhedron*, 2010, **29**, 391–399.
- A. G. Martynov, Y. G. Gorbunova, and A. Y. Tsivadze, *Dalt. Trans.*, 2011, **40**, 7165–7171.
- J. Mack and M. J. Stillman, 2001, **221**, 993–1032.
- M. Kasha, H. R. Rawls, and M. A. El-Bayoumi, *Pure Appl. Chem.*, 1965, **11**, 371–392.
- S. Yanagisawa, T. Yasuda, K. Inagaki, Y. Morikawa, K. Manseki, and S. Yanagida, *J. Phys. Chem. A*, 2013, **117**, 11246–53.
- F. Neese, *Wiley Interdiscip. Rev. Comput. Mol. Sci.*, 2012, **2**, 73–78.
- V. N. Nemykin, R. G. Hadt, R. V. Belosludov, H. Mizuseki, and Y. Kawazoe, *J. Phys. Chem. A*, 2007, **111**, 12901–13.
- V. N. Nemykin and J. R. Sabin, *J. Phys. Chem. A*, 2012, **116**, 7364–71.
- X. Cai, N. Sheng, Y. Zhang, D. Qi, and J. Jiang, *Spectrochim. Acta, Part A*, 2009, **72**, 627–635.
- L. Zhang, D. Qi, L. Zhao, Y. Bian, and W. Li, *J. Mol. Graph. Model.*, 2012, **35**, 57–65.
- S. O. Kang, J. M. Llinares, V. W. Day, and K. Bowman-James, *Chem. Soc. Rev.*, 2010, **39**, 3980–4003.
- A. G. Martynov, M. V. Panova, Y. G. Gorbunova, and A. Y. Tsivadze, *Macroheterocycles*, 2014, **7**, 47–54.
- A. G. Martynov, O. V. Zubareva, Y. G. Gorbunova, S. G. Sakharov, and A. Y. Tsivadze, *Inorg. Chim. Acta*, 2009, **362**, 11–18.
- N. Sheng, Y. Zhang, H. Xu, M. Bao, X. Sun, and J. Jiang, *Eur. J. Inorg. Chem.*, 2007, 3268–3275.
- G. R. Fulmer, A. J. M. Miller, N. H. Sherden, H. E. Gottlieb, A. Nudelman, B. M. Stoltz, J. E. Bercaw, and K. I. Goldberg, *Organometallics*, 2010, **29**, 2176–2179.
- X. Ling and E. Masson, *Org. Lett.*, 2012, **14**, 4866–9.
- F. Camps, J. Coll, and S. Ricart, *J. Heterocycl. Chem.*, 1983, **20**, 249–250.
- A. Y. Tsivadze, E. O. Tolkacheva, L. I. Demina, Z. G. Bitiev, and V. I. Zhilov, *Russian Federation Patent 2079499*, 1997.
- G. M. Sheldrick, *SADABS, Bruker AXS Inc.*, Madison, WI-53719, USA, 1997.

## Journal Name

59. SMART V5.051 and SAINT V5.00, Area detector control and integration software, Bruker AXS Inc., Madison, WI-53719, USA, 1998.
60. G. M. Sheldrick, *SHELXTL-97 V5.10*, Bruker AXS Inc., Madison, WI-53719, USA, 1997.
61. A. Schäfer, H. Horn, and R. Ahlrichs, *J. Chem. Phys.*, 1992, **97**, 2571.
62. F. Weigend and R. Ahlrichs, *Phys. Chem. Chem. Phys.*, 2005, **7**, 3297–305.
63. W. J. Hehre, *J. Chem. Phys.*, 1972, **56**, 2257.
64. J. D. Dill, *J. Chem. Phys.*, 1975, **62**, 2921.
65. M. M. Francl, *J. Chem. Phys.*, 1982, **77**, 3654.
66. R. Izsák and F. Neese, *J. Chem. Phys.*, 2011, **135**, 144105.
67. K. Eichkorn, O. Treutler, H. Öhm, M. Häser, and R. Ahlrichs, *Chem. Phys. Lett.*, 1995, **240**, 283–290.
68. K. Eichkorn, F. Weigend, O. Treutler, and R. Ahlrichs, *Theor. Chem. Acc.*, 1997, **97**, 119–124.
69. I. Horcas, R. Fernández, J. M. Gómez-Rodríguez, J. Colchero, J. Gómez-Herrero, and a M. Baro, *Rev. Sci. Instrum.*, 2007, **78**, 013705.